DEGREE PROJECT IN , SECOND CYCLE
STOCKHOLM, SWEDEN 2015

Fracture Simulation of Electrofusion Joining

AMIR ALIZADEH

KTH ROYAL INSTITUTE OF TECHNOLOGY

SCHOOL OF ENGINEERING SCIENCES

Abstract

Fracture Simulation of Electrofusion Joining

by Amir Alizadeh

This Master thesis investigates mechanical failures of electrofusion joints. This type of joints are used for weld high density polyethylene pipe systems where fitting and pipe will be welded together by the heat caused by the resistance of the copper cables to electric current. There have been some failures where a brittle crack has grown through the fusion zone. Polyethylene as a material has a ductile character but brittle behavior occurs due to an unsuccessful welding by a poor fusion interface.

In this study, we have chosen to investigate the plausible load cases that can cause the failure and studied the effect of the geometry of the fitting on the fracture toughness of the welded structure. We used the finite element method numerical analysis. We have approached unsuccessful welding (brittle) with a linear model and non-linear (CZM) model and successful welding (ductile) with a non-linear XFEM model. The material parameters needed for these models are gathered by series of experiments.

The results shows that the inside pressure is the critical load case. The linear model and CZM model are consistent in terms of predicted responses to the geometrical parameters for the unsuccessful welding. Decreasing the inner cold zone length, increasing the fusion length and the thickness of the fitting will improve the fracture toughness of the welded structure.

Sammanfattning

Fracture Simulation of Electrofusion Joining

av Amir Alizadeh

Detta examensarbete på masternivå handlar undersökning och simulering av brott i elektromuffsvetsar. Den här typen av svets används för att sammansvetsa rör av högdensitiets polyeten där muff och rör svetsas samman med värmen som skapas på grund av koppartrådens motstånd mot elektrisk ström. Flera tidiga brott där en spröd spricka har växt genom svetsområdet har observerats. Polyeten som material är duktilt men sprött beteende förekommer på grund av dålig svets och svetsgränssnitt.

I detta arbete valdes att undersöka de möjliga kritiska belastningar som kan orsaka brott och påverkan av muffens geometri på brottmotståndet hos den ihopsvetsade muff- och rörstrukturen. Den numeriska finita element-metoden användes.

En dålig svets (spröd) angreps med en linjär modell och en icke linjär (CZM) modell och en bra svets (duktil) hanterades med en icke linjär (XFEM) modell. Aktuella materialparametrar identifierades genom experiment. Resultatet visar att det inre trycket är den kritiska belastningen.

I termer av respons till de geometriska parametrarna, var den linjära och icke-linjära modellen (CZM) för den dåliga svetsen konsekventa. Reducerad inre kylzon, ökning av svetslängd, och ökning av mufftjocklek ökar brottmotståndet hos den ihopsvetsade strukturen.

Acknowledgements

I would like to express my gratitude to my supervisors Artem Kulachenko from Royal Institute of Technology and Daniel Ejdeholm from Swerea KIMAB for their support and engagement through this challenging and instructive master thesis. I like to thank 4S Ledningsnät for financing this project. Furthermore I want to thank Irene Linares Arregui for her help with experiments and laboratory work. I would like to thank PhD students and my class mates that never hesitated to spend time discussing my ideas and questions. Finally I want to thank my family for their unlimited support and love.

Contents

List of Figures

List of Tables

Abbreviations

HDPE	High Density Polyethylene
EF	Electrofusion
LEFM	Linear Fracture Mechanics
FEM	Finite Element Method
XFEM	Extended Finite Element Method
CZM	Cohesive Zone Method
HSR	High Stress Region
LSR	Low Stress Region
RSCG	Resistance to Slow Crack Growth
GFEM	Generalized Finite Element Method
PUM	Partition of Unity Method
SIF	Stress Intensity Factor
CMO	Crack Mouth Opening

Chapter 1

Introduction

1.1 Introduction

High density polyethylene (HDPE) is commonly used for the fabrication of gas and water pipes. Pipe systems contain a large number of pieces that need to be connected; therefore a joining process is unavoidable. There are different methods to connect (join) two pieces of pipes together such as butt welding, electrofusion, mechanical joining etc. In this study we will concentrate on electrofusion. This type of joining is expected to have a long life time functionality, however there have been a number of unexpected failures after a short period of time. In all the reported failures, the cracks have been propagating through the weld zone and the material failure at the crack surfaces has a brittle character even though HDPE is a ductile material. Earlier studies of the material characterization of the fusion zone revealed the signs of an unsuccessful welding process. The factors that affect the results are welding temperature, time, pressure and contamination of the welding surface. Most common mistakes happen during the installation which prevents a good flow of the melted material and the desired mixture of the PE chains. These mistakes include using a pipe where the exterior surface is unscraped or poorly scraped and low quality EF coupler that causes a low welding pressure. In both cases the overall joint is classified as bad welding [5].

Material parameters of the joining zone will be different from the original HDPE in both successful and unsuccessful joining. These differences are negligible in the first case but the variation is significant if the welding is not done correctly.

Knowledge of the reason behind the brittle character of the welding zone, the short life

expectancy and fracture through the welding zone guides this work towards investigation based in a functional numerical model which will be used to study the effect of the standard dimensions of the welding joints [6] during possible load cases, finding the important parameters for the EF fitting.

The models of the joining are created with the finite element method (FEM) using a commercial finite element code ANSYS. Three models will be used in this study: linear, non-linear with cohesive zone model and non-linear with the extended finite element method. The linear model is the first step of the simulation process where any non-linearity such as large or plastic deformation, creep, etc. is not included. A linear fracture mechanics (LEFM) analysis is done in this part and the stress intensity factors (SIF) K_I & K_{II} are calculated. Even though our material is non-linear, a linear model can provide us with valuable insights that can assist us both directly with the investigation and in designing the more complex non-linear models. In order to characterize the mechanical response and gather necessary material parameters for the model, series of experiments are designed and conducted.

1.2 Problem formulation and strategy

1.2.1 Problem formulation

The goals of this work are divided into the following points.

- Fining the critical magnitude of the load causing failure in case of successfull and unsuccessful welding.
- Verifying the SIS standard, $EN - 12201 - 3$.
- Determining the important geometric parameters and their contribution.

1.2.2 Execution

1. Literature study about the material and the joining, learning about the material and the fitting, finding load cases, etc.
2. Creating a simplified and linear model.
3. Parameter study.
4. Creating non-linear models.
5. Parameter study.

1.3 High Density Polyethylene (HDPE)

Manufacturing of HDPE started in 1950. The first generation had a very low comonomer content, very high density and low resistance to slow crack growth (RSCG). The second generation was improved by increasing the comonomer content which led to reduced density and increased RSCG. Finally the third generation (PE100) was manufactured through a bimodal technology with more resistance to hydrostatic pressure and excellent long term properties, such as RSCG.

HDPE has two molecule families, i) short and unbranched polymer chains which provide the high density (first polymerization) and ii) long and branched macromolecules that improved the RSCG (second polymerization). It is a semi-crystalline polymer with a density of 940-970 kg/m^3 and up to 80% crystallinity. Amorphous (non-crystalline) and high regularity (crystalline) areas are shown in Figure 1.1. The crystals are located where the polymer chains are folded in a lamellae of higher degree of order. Higher order of crystallinity will cause higher density, stiffness, hardness, tensile strength, creep resistance and resistance to chemicals but it will reduce permeability, RSCG and impact strength. HDPE is a visco-elastic material where the polymer chain length determines the level of viscosity [1].

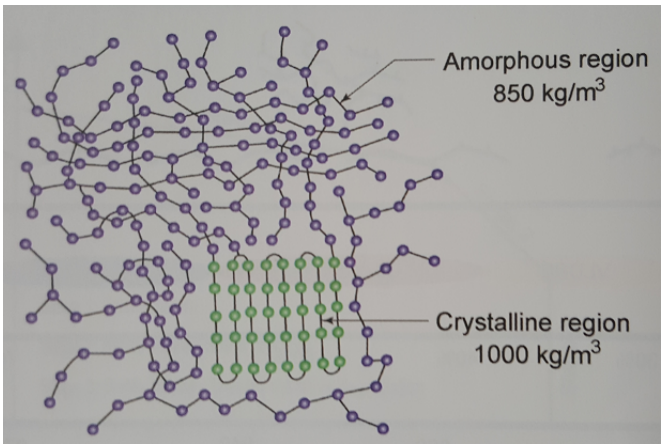

Figure 1.1: Amorphous and crystalline molecular regions in HDPE with their density contribution [1].

1.4 Electrofusion joining (EF)

Electrofusion joining is a method for welding PE pipe systems. The main idea is that the resistance in the wires which runs through the joint will generate enough heat to melt the material in fitting and pipe in the welding zone, Figure 1.2. The melted PE will expand up to 20% when the temperature rises from 20 to 200 °C. The cold zones stop the melted material from flowing out. The PE chains braid randomly together due to the internal flow and after the cooling time the two PE pieces, pipe and fitting, are welded as one [2].

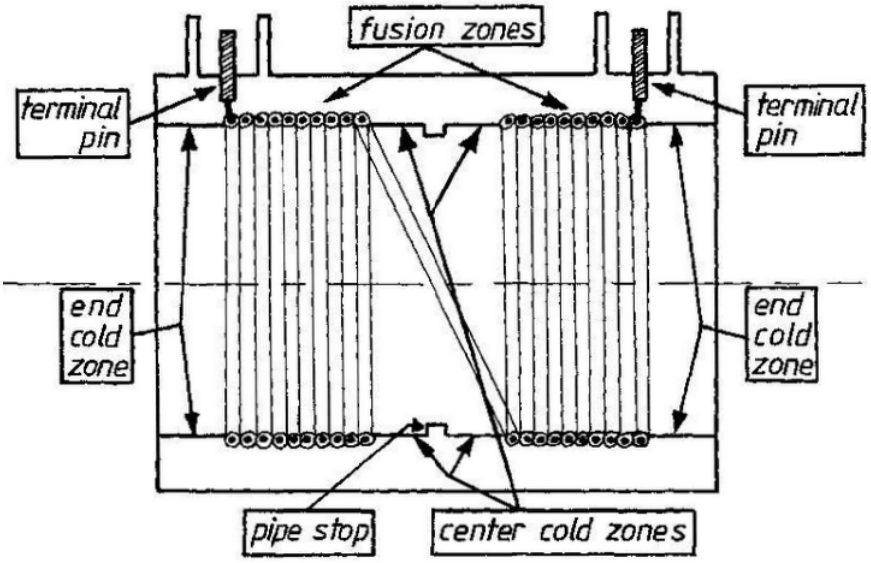

Figure 1.2: Electrofusion fitting [2].

1.5 Previous research

1.5.1 Effect of cooling time

Authors G. Ayoub et al. [7] have studied the effect of cooling time in the EF welding process. Under a bending load they have investigated fusion zone deformation, degree of crystallization, tensile creep strength and tensile fatigue strength for long time performance.

They observed that increasing the cooling time decreases the deformation and residual strain. The degree of crystallinity is increased but not significantly. There is no large fluctuation of molecular orientation and the material remains almost isotropic. The tensile strength nether is affected significantly with the cooling time. The long-term creep strength was different for low or high stress regions. In HSR the creep strength decreased with increase of cooling time but in LSR it was the opposite.

1.5.2 Defects and failures

Defects and failures in electrofusion fittings are categorized in a study preformed in 2011 [5]. Factors that define a successful process were determined to be welding temperature, time, pressure and welding surface conditions. The following problems are consequences of misapplying these factors.

- **Poor fusion interface**

  The reason for this phenomenon can be cold welding and/or contamination of the interface. All three named reasons above lead to brittle behavior of the material at the weld interface.

- **Voids**

  Voids can appear due to trapped air, shrinking during the cooling process or due to wet or unscraped welding surface. They create structural discontinuities in the EF joint and can initiate cracks.

- **Structural deformity**

  The EF joint fails to keep an expected structure after welding. The effects of this phenomenon are vertical dislocation of wires, misalignment and inadequate insertion.

- **Over welding**

  This is caused by excessively high temperature around the copper wires due to too high energy input and results in a brittle behavior during the peeling with a carbon-like dusty material on the surface.

Chapter 2

Analysis and Material model

2.1 Geometry

The axial and reflective symmetry of the joint makes it possible to consider only half of the cross section area using axisymmetric model as shown in Figure 2.1. To create the geometry we used dimensions of a manufactured fitting by AGRU based on the standards established by [6]. Even though the distance between two fittings can be around 100 meters, we assume that we can choose to have a shorter total length than the actual pipe length without significantly affecting the results. The maximum relative difference, Eq. 5.1, between 0.15 and 70 meters is approximately $5 \cdot 10^{-3}$ m as shown in the result section, Figure 5.3.

The copper wires have stiffness 60 to 70 times higher than the HDPE and are modelled as rigid inclusions.

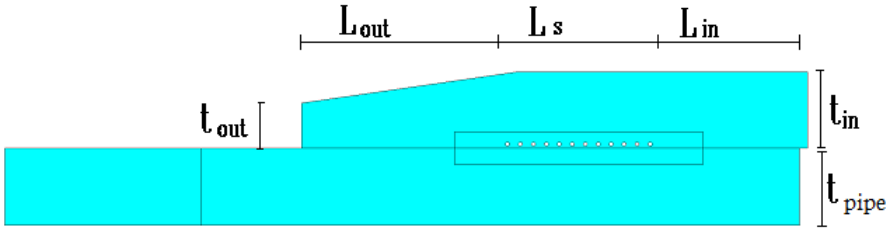

Figure 2.1: Geometric parameters.

2.2 Load cases

There are two main groups of loads: the loads during the installations and the loads under employment period, they are listed in Table 2.1, where we point out those which are relevant to this project. Some of these load cases affect the pipe system and are presented in P101[8] & P98[9] from Swedish water (Svenskt vatten). The exact loads that affect the joining are unknown. We have chosen to discount some of the cases shown below on account of their insignificant contribution to the joining itself.

Table 2.1: Load cases during installation and employment.

Load case	Installation	Employment	Accounted for
Tensile load	X	-	-
Ground load	-	X	X
Traffic load	-	X	X
Ground water Load	-	X	X
Inner pressure	-	X	X
Temperature load	-	X	X

The tensile load occurs during installation of pipes when they are dragged beneath the ground surface or in already existing pipe systems which is not the installing method of the reported failed EF fittings and therefore is not included in this study.

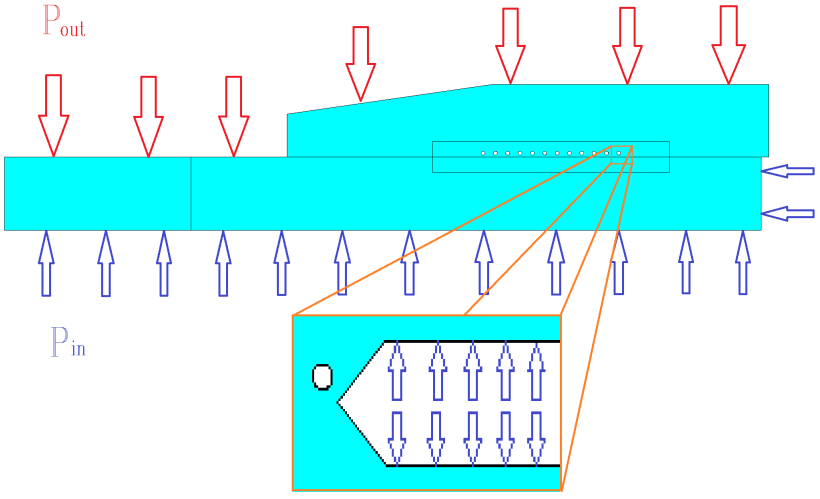

Figure 2.2: Structural load case.

The outside pressure is caused by the mass of soil above, traffic and ground water is then merged as one and is presented as a constant pressure on the outside of the pipe system.

The inside pressure will be applied as a constant value. Free buckling of circular cross

section is not of interest in this study because the stiffness of the pipe is much higher at the fitting and any possible buckling/ovalization happening away from the fitting was assumed to be irrelevant to this study.

The inside temperature will be set as constant but the outside temperature will vary depending on the depth where pipes are buried. Same depth in different parts of Sweden can have different temperatures.

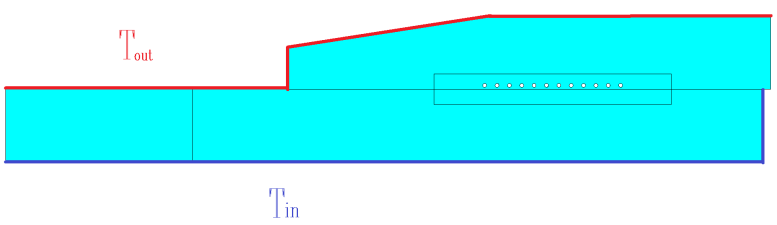

Figure 2.3: Thermal load case.

As mentioned above we have both structural and thermal loading. The thermal and structural loads applied to our model are shown in the Figures 2.3 & 2.2. We preformed the thermal analysis in a sequential uncoupled manner. The contribution is applied as nodal force in the structural analysis after it has been calculated as a degree of freedom in the thermal analysis, Figure 5.1.

2.3 Boundary conditions

Having the load cases and the geometry, the symmetric boundary conditions are applied in the model as presented in Figure 2.4, where no displacement in Y direction is permitted at the edges.

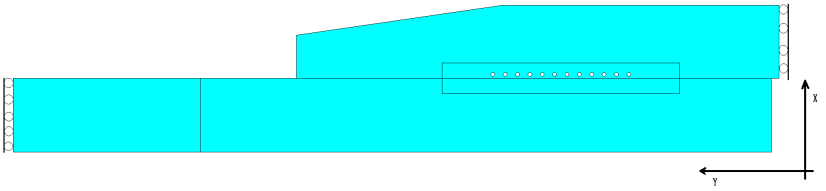

Figure 2.4: Boundary conditions.

2.4 Constitutive law

Deformation of a body contains two parts. The first part is reversible elastic and the second part is a permanent plastic deformation. The total strain and the transition from elastic to plastic deformation is presented in Eq. 2.1 to Eq. 2.3. E is the elastic modulus and H is the plastic modulus. [10]

$$\epsilon_{ij} = \epsilon^e_{ij} + \epsilon^p_{ij} = \frac{\sigma_{ij}}{E} + \frac{\sigma_{ij}}{H} \tag{2.1}$$

$$f(\sigma_{ij}, \sigma_f(\sigma_{Yield})) = \sigma_{effective}(\sigma_{ij}) - \sigma_f \tag{2.2}$$

$$\epsilon^p_{ij} = \begin{cases} 0 & f < 0 \\ \frac{\sigma_{ij}}{H} & f > 0 \end{cases} \tag{2.3}$$

When the effective stress reaches the yield criteria, Eq. 2.2, the plasticity will begin which is shown in Eq. 2.3.

2.5 Cohesive zone

A phenomenon in fracture mechanics is that at the very end of the crack tip there is an area called the cohesive zone, Figure 2.5. Considering an open crack, there is no stress on the crack interface (free surface) except in the cohesive area. The material connecting to the surfaces and the internal forces resist the crack opening and generate stress. The crack will further propagate when the stress level reaches the critical value.

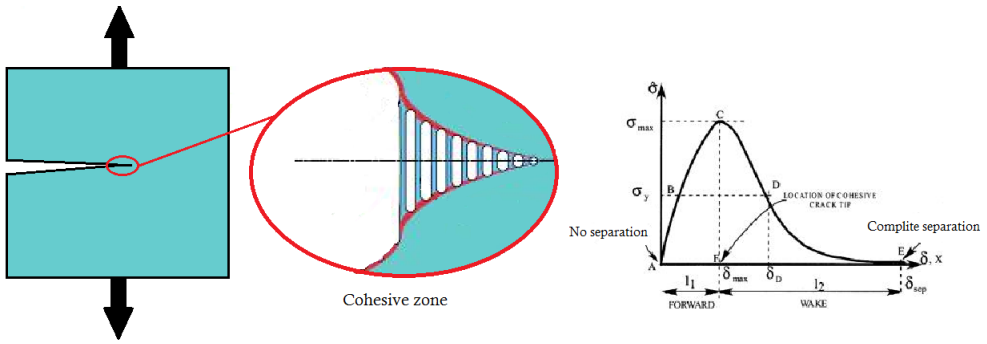

Figure 2.5: Cohesive zone [3].

2.6 XFEM, Extended Finite Element Method

The Extended Finite Element Method (XFEM) is used to model cracks and other discontinuities,[11], without the necessity to specify the predefined crack path as required in the CZM approach. The crack path will be predicted by the method. It is based on the generalized finite element method (GFEM) and the partition of unity method (PUM). It differs from basic FEM by the enriched degrees of freedom in the model with additional displacement functions that account for the jump in displacements across the discontinuity that is shown in Eq. 2.4.

$$u^h(x) = \sum_{i=0}^{I} N_i(x) u_i + \sum_{i=0}^{I^*} M_i(x) a_i \tag{2.4}$$

- $u^h(x)$: Approximated function,
- $N_i(x)$: Standard FE function of node i,
- u_i: Unknown of the standard FE part of node i,
- I: Set of all nodes in the domain,
- $M_i(x)$: Local enrichment function of node i,
- a_i: Unknown of the enrichment at node i,
- I^*: Nodal subset of the enrichment,

Chapter 3

Fracture Mechanics Analysis

3.1 Linear analysis

Material behavior and fracture mechanics of HDPE are non-linear by nature. Sometimes due to some material behavior like fragility (brittle material) and geometry shapes and dimensions, a linear approach can be provided with relatively good results and has a considerable advantage of being fast. Even if the linear analysis may not be appropriate for this problem, it is a good basis for a subsequent more complex and more sophisticated non-linear model. One other advantage is that the linear model can determine whether certain load cases, geometry shapes, etc. can be simplified or not. In the linear model, all non-linear phenomena like creep, hardening, cohesive behavior, large deformations, etc will not be considered.

Time dependent temperature and rate dependent parameters will be assumed as constant and a static analysis is chosen in this model. A 2D axisymmetric geometry that is shown in Figure 2.1 with the boundary conditions presented in Figure 2.4 will be used.

3.1.1 Material type & constitutive law

Even though the HDPE pipes are extruded as mentioned, the material around the fusion zone can be seen as isotropic [7]. This area is the most interesting region of our model and it is assumed that the rest of the geometry is isotropic as well.

The assumption of small deformation is fundamental in linear analysis. Plastic deformation is a non-linear behavior and therefore not included in the linear model. The plastic part of Eq. 2.1 will be ignored and all deformations will obey Hook's law, Eq.3.1.[10]

$$\epsilon_{ij}^{e} = \frac{1}{2G}(\sigma_{ij} - \frac{\nu}{1+\nu}\delta_{ij}\sigma_{kk}) + \delta_{ij}\alpha\Delta T \tag{3.1}$$

Where G is the Shear modulus, ν is the Poisson's ratio and α is the Thermal expansion factor.

3.1.2 Stress intensity factor & LEFM criteria

In Eq. 3.2 to 3.4 we define some of the key conceptions in fracture mechanics that are essential in this part of the project. K_I to K_{III} are stress intensity factors (SIF), G is the energy release rate that refers to energy needed to open a crack and J is called conservation law.

$$\bar{K} = \lim_{x \to +0} \bar{\sigma}(x, 0)\sqrt{2\pi x} \tag{3.2}$$

$$G = \frac{K_I^2}{E'} + \frac{K_{II}^2}{E'} + \frac{(1+\nu)K_{III}^2}{E} \tag{3.3}$$

$$J = \int_C (W'\delta_{1j} - \sigma_{ij}u_{i1})njdC \tag{3.4}$$

When it comes to linear fracture mechanics (LEFM) an assumption is made that G is equal to J and crack propagation will occur when K_i reaches the critical value, $K_{i,c}$ [12].

3.1.3 Discretization

We need to discretize the geometry and create small elements in order to use a numerical approach such as FEM. The element number, size and number of nodes per element will affect the results. Finer discretization will make the model more accurate, but at the same time increases the computational time. Therefore is important to plan a strategy for discretization and have finer division in areas of interests, which is the welding zone in this case, and more coarser in others. This is another reason why we model the copper wires as rigid inclusions to minimize the number of elements as much as possible, Figure 3.1.

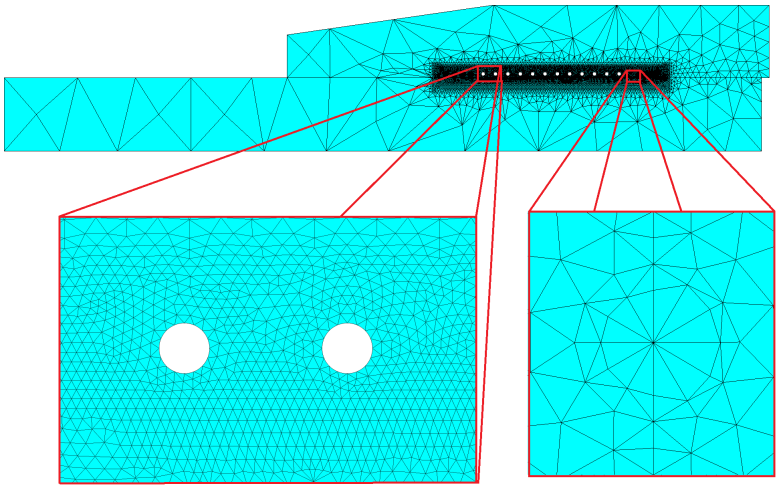

Figure 3.1: Discretization in the linear analysis.

Element types differ by shape functions that couple the nodes of the elements, numbers of the nodes in each element and DOF at each node. A greater number of nodes will provide results closer to a continuous solution. However, a higher number of nodes and DOF will lead to a higher number of equations to be solved and therefore will require more calculation resources.

Figure 3.2 shows an axisymmetric plane element with 8 or 6 nodes that has two DOFs at each node that is chosen for the 2D geometry of the linear model.

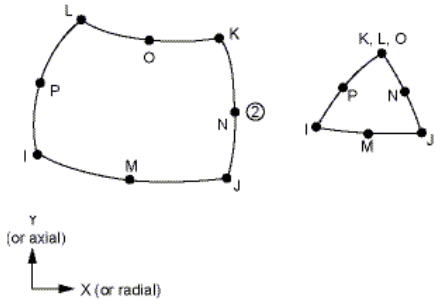

Figure 3.2: 8-node axisymmetric element with alternative for collapsed side.

3.2 Non-linear analysis

The non-linear model will include the non-linear behavior of the material like plasticity, large deformation, creep, etc.

The non-linear analysis allows for simulation of crack propagation. The successful and unsuccessful welding will be modelled with extended finite element method (XFEM) and cohesive zone method (CZM) respectively. The reason behind the choices of these two different methods is the fracture behaviors of the cases. In the case of successful welding the crack propagation path is unknown, as opposed to unsuccessful fusion and therefore the XFEM is more suitable for this task. The CZM require a predefined propagation path which makes it suitable for the case of unsuccessful welding where the weakest direction is known.

In a non-linear model there is no need for calculating SIFs. To compare and investigate the results of the non-linear parameter study we can use the critical load that causes the crack initiation, which is a more relevant parameter in any case. Computing the full crack growth is required in either case.

3.2.1 Crack simulation with CZM

In CZM method the crack path should be predefined. The strength at the crack surface will be defined by a cohesive relation for example bilinear, exponential, etc. that will govern the condition at which the crack growth occurs. This property makes the method suitable for an unsuccessful welding when the crack propagates though the welding zone and the path is known.

A 2D axisymmetric geometry is allowed in this method. The same geometry and element types applied in the linear analysis can also be used. The difference is that fitting and pipe are created as two separate geometries that are connected together with a defined bilinear cohesive condition along the welding, Figure 3.3.

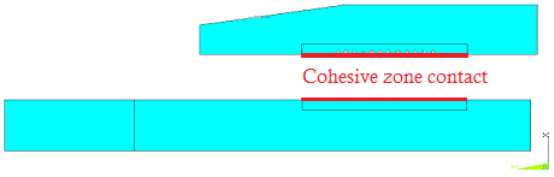

Figure 3.3: Cohesive zone contact in the 2D CZM-model.

3.2.2 Crack simulation with XFEM

Assuming that the welding zone will have the same properties as the HDPE material after successful fusion will result in an unknown crack path that will depend solely on the load and geometry. There is no need for predefined crack interface in this method. The crack will propagate in the direction where circumferential stress is evaluated at its maximum in every sub-step during simulations. That will be the direction where K_I is largest and a cohesive relation will be defined for the material that decides the strength of the surface where the crack propagates. The material parameters such as Young modulus, yield stress and maximal stress will be determined by experiments.
By expanding the geometry in circumferential direction a 3D body is created. The reason for increasing the dimension of the geometry is that no 2D axisymmetry element is available for XFEM simulation. Pipe and fitting will be designed as one body as it is shown in Figure 3.4.

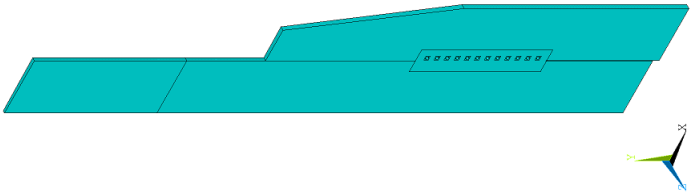

Figure 3.4: 3D geometry in XFEM simulation.

The designed 3D body will require new cyclic-symmetric boundary conditions in circumferential direction. The element that is used is an 8 node 3D solid element, suitable for creep and large deformations where the nodes have 3 transient DOF, shown in Figure 3.5.

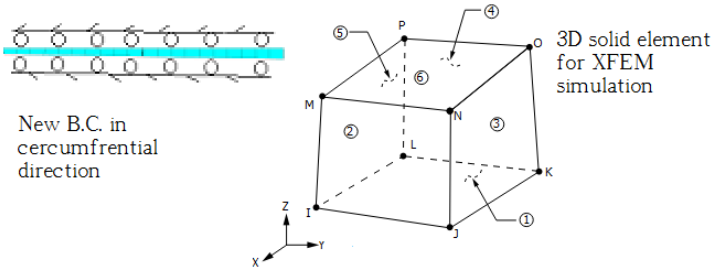

Figure 3.5: Circumferential boundary conditions (B.C.) and XFEM element.

An initial crack direction should be defined for the simulation. The region covered by enriched finite elements needed for XFEM should be limited for the sake of computational efficiency. This is the reason that only the area around the welding zone is chosen for enrichment. We have prescribed load and if the crack starts to grow it will continue propagating. In Figure 3.6 the discretization and the initial crack direction are presented.

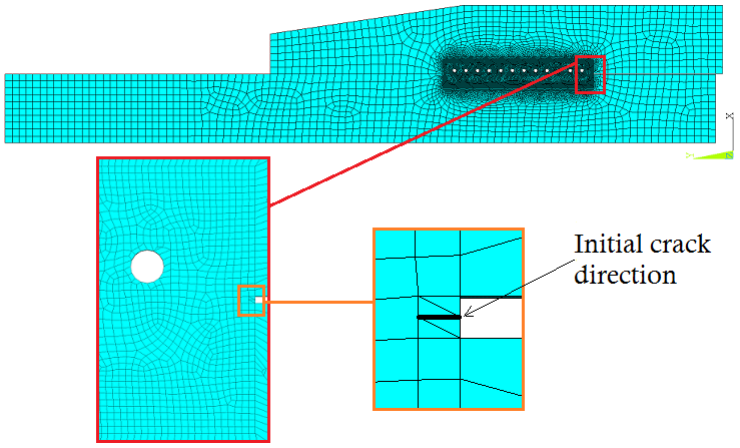

Figure 3.6: Discretization and initial crack direction.

Chapter 4

Experiments & Input data

4.1 Experiment

In order to create numerical models, especially the non-linear ones, we have thoroughly to characterize the material behavior of HDPE. The linear analyses requires only elastic properties, which can be found in the literature. It is more complicated when it comes to behaviours like plastic deformation, cohesive zone relation, etc where, the data suitable for the model is missing. Therefore, this challenge of collecting the required input data is approached by designing series of experiments. The material properties collected from these tests will provide strain vs. stress relation and the temperature effect on the material parameters. Another purpose with the experiments is to determine the tensile and shear strength of the welding zone in the case of successful and unsuccessful fusion.

4.1.1 Tensile experiment

The tensile test with the setup shown in Figure 4.1 is chosen for investigation of the following matters.

- Stress and strain relation for elastic-plastic deformation of HDPE.
- Temperature dependency of deformation behavior of HDPE in temperatures 10 °C and 25 °C.
- Interface strength of a successful and unsuccessful weld.

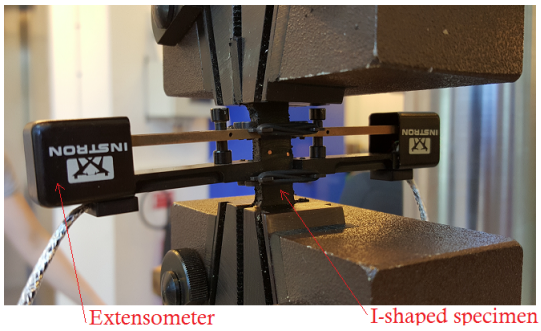

Figure 4.1: Setup for the tensile test.

I-shaped specimens used for the tensile tests are shown in Figure 4.2 and are divided into three groups. The first group of specimen is made from the pipe material only. The second and third group are specimens that are created from successful and unsuccessful EF welds (pipe & fitting) respectively.

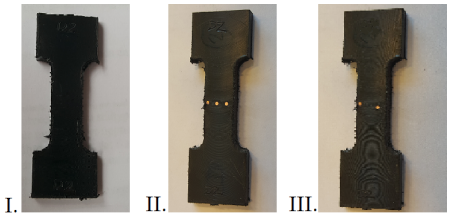

Figure 4.2: Three groups of specimens for the tensile test.

For the tensile test on the pipe material in 10 °C, the specimen was isolated from the environment. A supervised flow of cold air was sent in to the container and the temperature was kept at 10 ± 1 °C as it is presented in Figure 4.3.

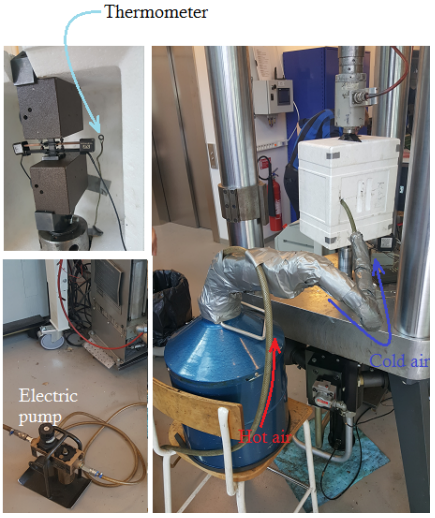

Figure 4.3: Setup for the tensile test in temperature of 10 °C.

The loading in the tests is prescribed displacement with a constant rate. The force, time, grip and extensometer displacement are gathered during each experiment. Unfortunately the extensometer has a limited range and therefore has to be removed in the middle of the test. The grip displacement contains both specimen and grip deformation. To find the specimen deformation after the extensometer is removed , the grip deformation needs to be eliminated from the total displacement. It is assumed that the grip will only have an elastic and linear deformation and consequently the extensometer's displacement can be calculated by Eq. 4.1.

$$\delta_{extensometer} = (\delta_{grip} - C \cdot F) \cdot \frac{L_{extensometer}}{L_{specimen}} \tag{4.1}$$

Where δ is deformation, L is length and C is the grip compliance which needs to be determined before Eq. 4.1 can be used. True stress and true strain for each test is calculated with Eq. 4.3. [13]

$$\epsilon_{eng} = \frac{\delta_{Extensometer}}{L_{extensometer}}, \quad \sigma_{eng} = \frac{Force}{A_0} \tag{4.2}$$

Where A_0 is the initial cross section area.

$$\epsilon = \ln(1 + \epsilon_{eng}), \quad \sigma = \sigma_{eng} \cdot (1 + \epsilon_{eng}) \tag{4.3}$$

4.1.1.1 Tensile experiments results

The material behaviors observed during the experiments of specimens from the joining were consistent with expectations. The successful welding tests had ductile failures with higher maximum stresses compared to the unsuccessful ones that failed in a brittle manner. In Figure 4.4, both cases are presented.

With the help of Eq. 4.1 the grip compliance and the deformation after extensometer removal were calculated. Next step is to calculate the stress and strain for every test value (for each test). Eq.'s 4.2 & 4.3 will be used for this matter. To illustrate these operations one of the specimens was chosen and the results of each step are presented in Figure 4.5.

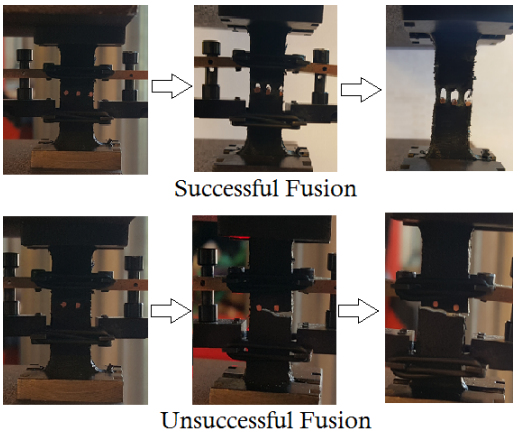

Figure 4.4: Tensile test of successful and unsuccessful fusion.

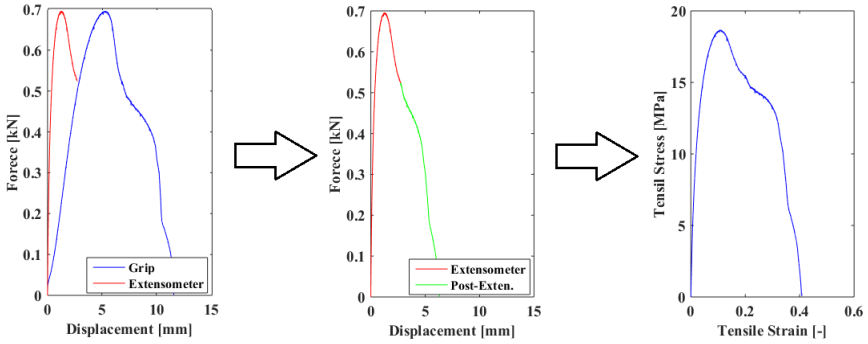

Figure 4.5: An example of data from successful weld test before and after implementing Eq. 4.1 and stress vs. strain calculated by Eqs. 4.2-4.3.

In Figure 4.6 the graphic results of all tests are presented. As it can be observed the variation of gathered data is unnoticeable in the cases of successful welding, I, in contrast to unsuccessful ones, where it is very large, II. In Case III the results of material behavior as function of temperature is compared. The result from room temperature test shows a lower maximal stress and stiffness but higher elongation before total fracture in comparison with the test done at 10 °C.

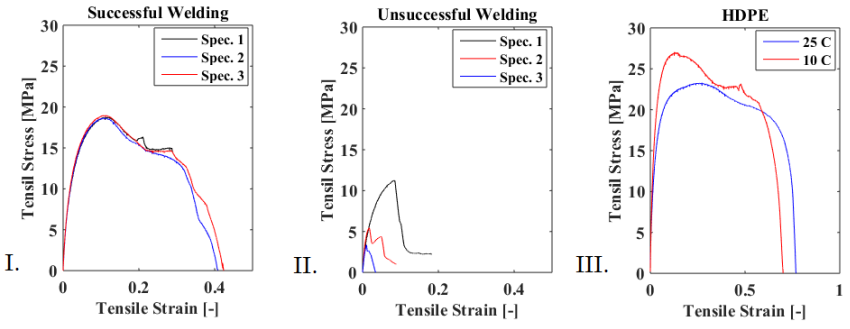

Figure 4.6: Graphical presentation of the tensile experiment results from the "Good" welding (left), "Bad" welding (middle) and HDPE pipe material (right).

In each case the Young's modulus is calculated as the slope of the fitted line to the beginning part of every curve where the behavior is most linear. The yield stress is chosen to $Rp_{0.02}$ value and it is the stress where a linear unloading would give a plastic strain, $\epsilon_{plastic}$, equal to 0.02%. This value is gathered for all these cases to illustrate the similarities and differences. For two tests of unsuccessful fusion the fracture occurs before the plastic strain reached 0.02, therefore no yield stress is calculated for these tests.

One should keep in mind that the HDPE pipes are extruded and polyethylene chains have orientation along the axial direction as opposite to the welding zone that has a more isotropic characteristic. This can be seen clearly when the cases $I\&III$ are compared in terms of elastic response. The parameters gathered and calculated from the tensile experiments are presented in Table 4.1.

Table 4.1: HDPE tensile experiment results.

Successful Welding		Unsuccessful Welding		HDPE	
$\sigma_{max,spec.1}$	$18.71[MPa]$	$\sigma_{max,I}$	$11.27[MPa]$	$\sigma_{max,10}$	$26.51[MPa]$
$\sigma_{max,spec.2}$	$18.57[MPa]$	$\sigma_{max,II}$	$5.46[MPa]$	$\sigma_{max,25}$	$22.08[MPa]$
$\sigma_{max,spec.3}$	$18.95[MPa]$	$\sigma_{max,III}$	$3.36[MPa]$	-	-
$E_{spec.1}$	$1.28[GPa]$	$E_{spec.1}$	$0.48[GPa]$	E_{10}	$1.58[GPa]$
$E_{spec.2}$	$1.03[GPa]$	$E_{spec.2}$	$0.61[GPa]$	E_{25}	$1.14[GPa]$
$E_{spec.3}$	$1.26[GPa]$	$E_{spec.3}$	$0.65[GPa]$	-	-
$\sigma_{Y,spec.1}$	$12.57[MPa]$	$\sigma_{Y,spec.1}$	$8.68[MPa]$	σ_{10}	$19.75[MPa]$
$\sigma_{Y,spec.2}$	$13.26[MPa]$	$\sigma_{Y,spec.2}$	-	σ_{25}	$15.62[MPa]$
$\sigma_{Y,spec.3}$	$13.09[MPa]$	$\sigma_{Y,spec.3}$	-	-	-

4.1.2 Shear experiment

It is difficult to achieve pure shear state in the experiment. In the attempt to create a pure shear case a setup and specimen that are shown in Figure 4.7 and 4.8 were designed. The setup transfers the vertical motion of the grip to one side of the specimen and creates a rigid body motion while the other side stays in place. This creates a shear loading at the smaller part of the specimen. It is no longer possible to use extensometer to gather data and the only data gathered from the experiment are force and grip displacement. This problem requires another way to gather the specimens deformation in order to calculate the grip compliance. To capture the specimen's deformation, several horizontal lines were marked on the specimens and pictures were taken during the test, Figure 4.7.

The goal was to measure the deformation of these lines on the specimen in the pictures.

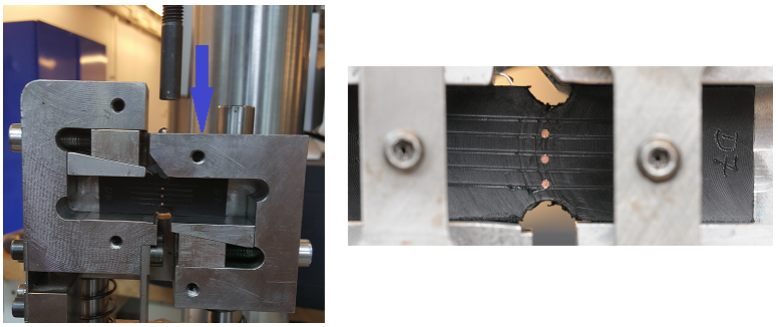

Figure 4.7: Setup for the shear experiment (left) and horizontal lines for capturing specimen deformation, (right).

It was assumed that there would be no deformation in the rigid part of the specimen and the force is transferred to the middle section. This force applied on the cross section area A_0 is the shear stress. To calculate the shear strain, γ will be calculated by Eq. 4.4.

$$\tau = \frac{Force}{A_0}, \quad \gamma = \arctan(\frac{\delta}{t}) \tag{4.4}$$

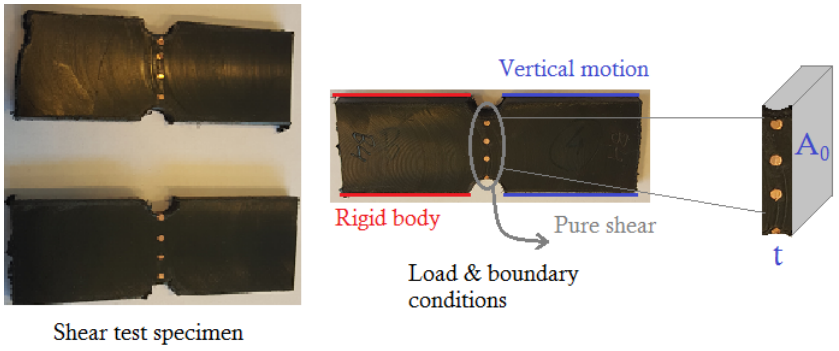

Figure 4.8: The shear test specimen and boundary conditions applied during the test.

4.1.2.1 Shear experiments results

In Figures 4.10 & 4.9 images of the deformation of a successful and an unsuccessful weld from the initial state until a crack appears is illustrated. It can be observed that the specimen is more deformed in the case of successful fusion before the crack initiates, and the crack does not have the same brittle character as the unsuccessful one.

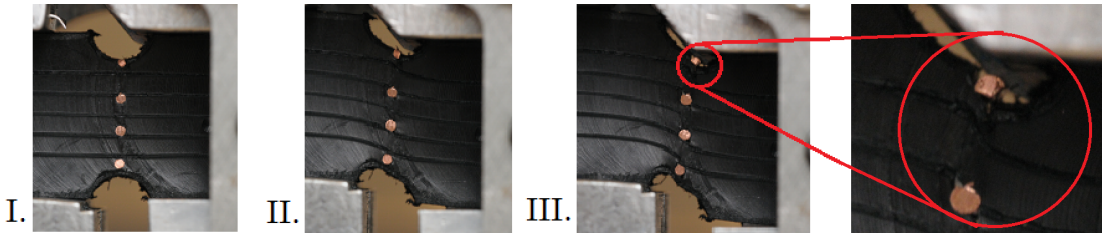

Figure 4.9: Shear experiment on specimen from a successful fusion.

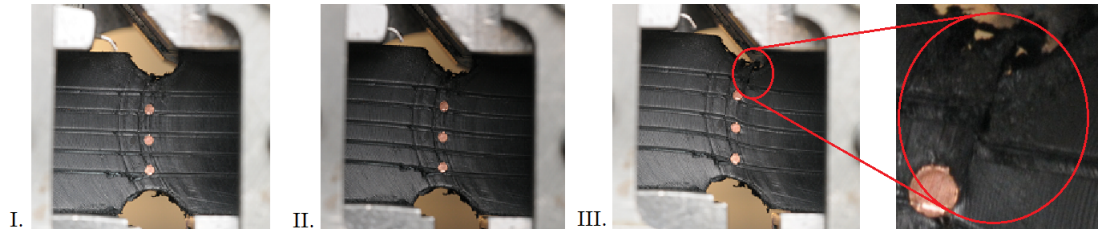

Figure 4.10: Shear experiment on specimen from an unsuccessful fusion.

Unfortunately the design chosen for the shear experiment could not contribute with information useful for the models. There were three main issues that made this design unsuccessful. First, the drawn horizontal lines that were supposed to assist in finding the grip compliance and scale the total deformation to specimen deformation, proved to ineffective. Second, it was not possible to perform any of the experiments completely when the specimen came in contact with the grip setup and prevented correct data due to the large deformation ability of HDPE. Third, during some of the experiments it was noticed that the whole middle section rotated as a rigid body which led to a state very different from pure shear. What was obvious however, the poorly welded interfaces showed considerable resistance to shear. Together with the fact that the shear force is not the dominant in the considered load cases, the failure due to shear is very implausible even for the unsuccessful weld.

4.2 Geometric, material parameters & load values

The geometric parameters were collected from a fitting produced by the company AGRU as mentioned earlier in the Geometry Section, 2.1. The standard relation between inner pressure and dimension of the pipe is shown in Figure 4.11, where SDR value is the fraction between diameter and thickness of the pipe and C_1 & C_2 are safety factors of 1.25 and 1.6,[9]. To estimate the surrunding pressure on the pipe system it was assumed that the pipe had to be at the depth of 2 m under ground where the temperature is around 4 °C, normal depth of ground water level is found to be approximately 1.5 m below surface and the traffic contribution to be a point force of 10 kN directly above the joint. The thermal material parameters and poisson's ratio are gathered from a manual published by SIMONA, [14].

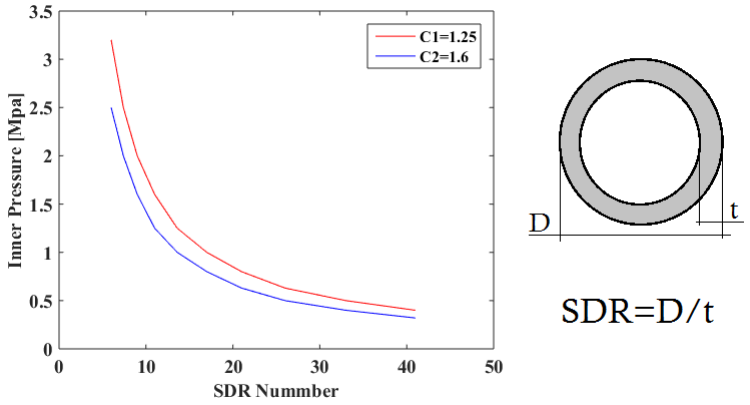

Figure 4.11: Inner pressure as a function of SDR value with two safety factors C_1 & C_2.

For the tensile modulus of elasticity, E and yield stress for HDPE (PE100) the use of the results of the tensile experiment of the successful welding was chosen. Even though the values of tensile modulus, maximal and yield stress were lower than the test results from the experiment on pure HDPE material (pipe), they were presented in a more complete format suitable for the model. First of all, an isotropic assumption was made. The pipe had an orientation along the axial direction that was mentioned earlier and therefore had higher strength. The second reason is that the area of interests where the mechanical and fracture properties will be studied is the fusion zone.

Investigating the result of the tensile test in 25 °C and 10 °C, it can be observed that the changes in parameters are not insignificant. Therefore it is necessary to find the correct parameter values in order to maintain the validity of the model and minimize the error.

The perfect situation would be if the tests are performed in temperature to which the pipe systems are exposed to but the hindrance is that these types of experiments are complicated and require time and resources.

The article on temperature effect on tensile properties of HDPE [15] by N. Merah et al. shows a linear dependency of Young's modulus and yield stress on temperature, therefore linear relations between parameters from the two tests on the HDPE pipe material in different temperatures were calculated. Parameters of the welded material were assumed to change with the same rate as pipe material. The only parameter assumed to be independent of temperature change is surface strength, σ_{max}, in case of unsuccessful fusion.

The geometric dimensions, material parameters and other values chosen to use in the models are presented in Table 4.2.

Table 4.2: Input data for HDPE pipe and fitting.

Name	Value	Name	Value
L_{in}	$18 \cdot 10^{-3}[m]$	Thermal conductivity	$0.38[\frac{W}{m^{\circ}\mathrm{C}}]$
L_{out}	$24 \cdot 10^{-3}[m]$	Thermal expansion	$1.3 \cdot 10^{-4}[\frac{1}{^{\circ}\mathrm{C}}]$
L_s	$21 \cdot 10^{-3}[m]$	Yield stress (SW)	$18.22[MPa]$
t_{in}	$9.6 \cdot 10^{-3}[m]$	E (SW)	$1.55[GPa]$
t_{out}	$5.6 \cdot 10^{-3}[m]$	$\sigma_{max,SW}$	$23.88[MPa]$
d_{cable}	$1 \cdot 10^{-3}[m]$	$\sigma_{max,UW}$	$3.36[MPa]$
t_{pipe}	$5.45 \cdot 10^{-3}[m]$	Contact stiffness (SW)	$123.64[\frac{GPa}{m}]$
P_{out}	$40[kPa]$	Contact stiffness (UW)	$93.56[\frac{GPa}{m}]$
P_{in}	$3.2[MPa]$	ν	0.38
T_{out}	4[°C]	-	-
T_{in}	10[°C]	-	-

Chapter 5

Results, Discussion & Conclusions

5.1 Results & conclusion of the linear simulation

Stress intensity factors, K_I and K_{II} are the values that were calculated for comparison of the results during the parameter study with the linear fracture mechanic simulations. The results are presented through calculated relative difference with respect to the reference case, Eq. 5.1, where the "actual" value is the SIF value calculated with the original geometry and parameters.

5.1.1 Temperature distribution

After applying the thermal load and performing the thermal analysis, the results were transferred to the structural analysis. Practically the calculated temperature distribution was introduced as the thermal body load in the structural analysis. The resulting temperature distribution through the fitting and pipe when the outside temperature is at 4 °C and the inside temperature is at 10 °C, is shown in Figure 5.1.

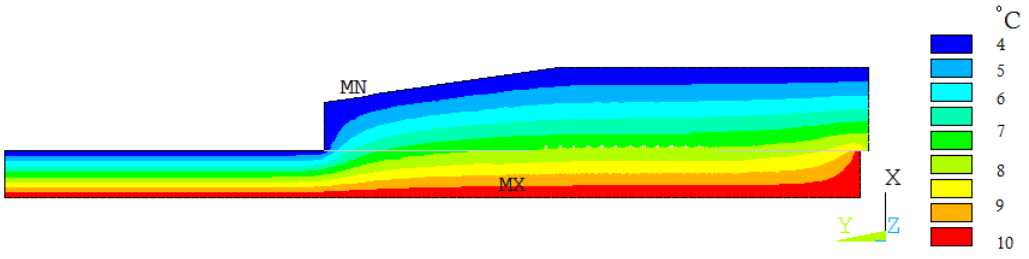

Figure 5.1: Temperature distribution through the joint.

5.1.2 Deformation and stress distribution

The temperature distribution, inner pressure and the outside pressure will deform the body and generate a stress distribution. The cold zones will act as crack mouth and the applied loads, especially the inner pressure, will be opening the crack. In Figure 5.2 an illustration of the distribution of von Mises effective stress and the deformation of the fitting is shown.

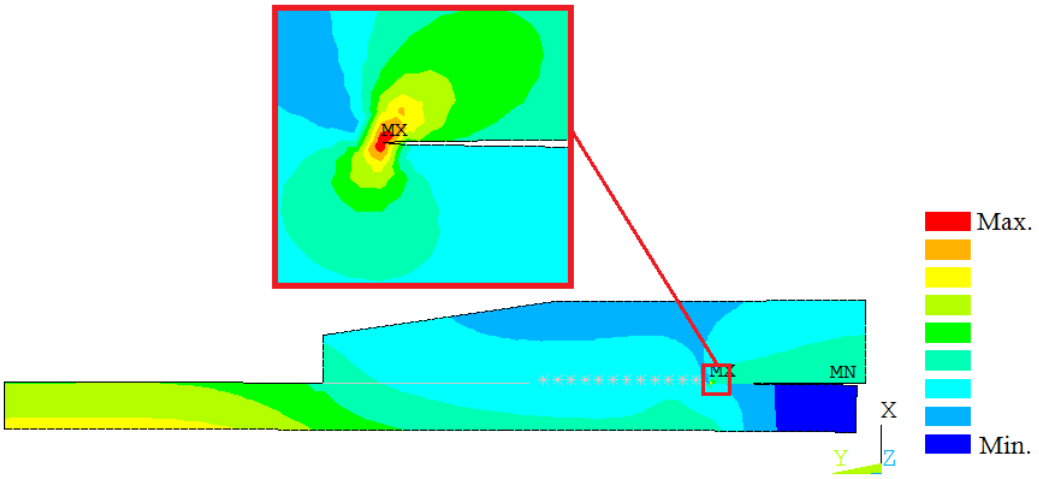

Figure 5.2: Deformation and effective stress distribution. A singularity in the stress field can be observed at the crack tip.

The first observation is that the inner cold zone has been opened due to applied loads and BC's but not the other cold zone. The main reason behind this is the inner pressure which forces itself inside the inner cold zone and pushes the pipe and fitting away from each other. So if a failure occurs it will start from the inner crack zone and therefore we calculate the SIF's for the inner cold zone. The second observation is the singularity is the stress distribution field at the crack tip, which is purposely created in linear analysis. Although the stresses are unreliable and are not used for comparison, the computed stress intensity factors are the factors to rely on.

5.1.3 Pipe length

It was mentioned earlier that a total length of 0.15 m was chosen instead of the actual length of the pipe. It is necessary to make sure that this simplification does not affect the outcome (in this case SIF's) more than an acceptable value. The K_I and K_{II} values were calculated as functions of the pipe length for pipe length between 0.15 and 70 m. The relative difference is calculated by following the Eq. 5.1.

$$\epsilon_i = \frac{Value_i - Value_{Actual}}{Value_{Actual}} \tag{5.1}$$

Figure 5.3 (Left) shows the difference as a function of total length to be in a range of 0 to 3 % and it can be observed that the difference is almost zero at the length of 10 m. The small magnitude of difference asserts that changing the pipe length from 70 to 0.15 m will not influence the results significantly.

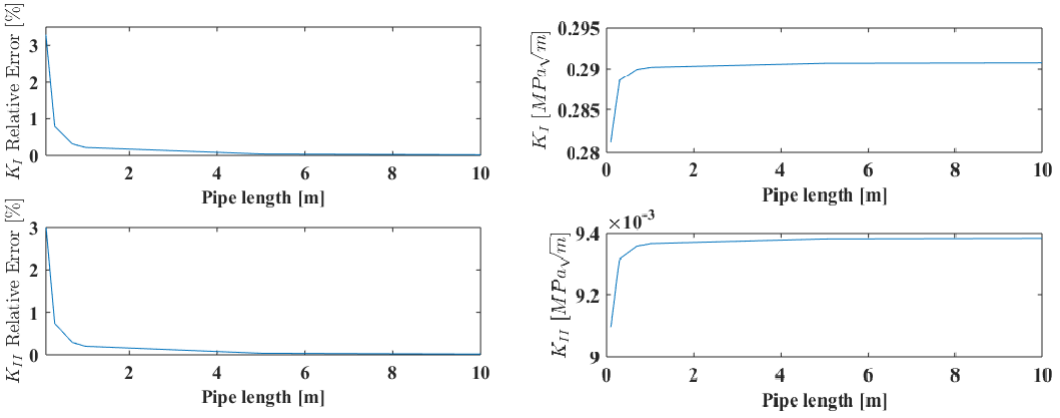

Figure 5.3: Relative difference as a function of pipe length (left) and K_I and K_{II} values as function of pipe length (right).

Beside the fast decreasing difference, it can be noted that K_I (opening mode) is the dominant SIF in this scenario.

5.1.4 Geometric & material parameter study

The geometric and material parameters as well as load cases can have a considerable impact on fracture mechanical qualities (in this case, SIF's) and therefore it is necessary to investigate the variation of the results due to the change of these parameters. This will assist in evaluating the model's sensitivity to these parameters and aid the verification of the standard[6]. In following sections we present the effect of varying the parameters

like welding and cold zone length, etc on the SIF. It should be mentioned that the total length of the fitting is kept constant.

First, we consider how the SIF's value behave if the crack starts to propagate through the fusion zone. This type of failure has been occurred in cases when the welding has been unsuccessful. In Figure 5.4 there is an illustration of the variation of K_I and K_{II} as the crack propagates straight through the welding zone. The variation of SIF values have been investigated both with and without the copper wires (rigid holes in this model) in the fitting.

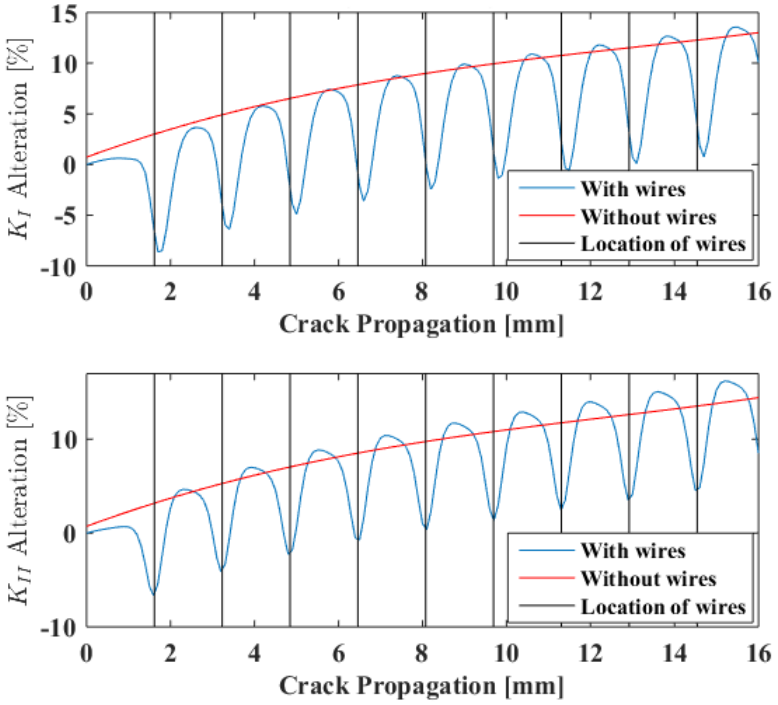

Figure 5.4: Relative difference of K_I and K_{II} as the crack length is extended (crack tip propatates) through the fusion zone.

The alteration of the SIF's is calculated by Eq. 5.1 with respect to the original geometry. The positive values indicate an increase and the negative values indicate a reduction of SIF magnitude. It can be seen that the mean value of SIF's increases with growing crack. The changes have an oscillating nature because of the electrical wires, which decrease the stress intensity if the crack aligns with their locations. This oscillatory behavior is not seen when the wires are removed from the geometry. It can be noted that removing the copper wires does not affect the initial SIF values significantly when the crack is located some distance away from the first wire.

Increasing the fusion length without changing the total and the outer cold zone length is in other words decreasing the crack length. In Figure 5.5 a plot of the SIF's as a

function of inner cold zone length is shown. The results indicate that the SIFs values are proportional to the length of inner cold zone in the case of prescribed force. A smaller inner cold zone results in i) a smaller area for inner pressure to act on that means lower force that opens the crack and ii)a minor lever which decrease the moment at the crack tip. This means that with smaller inner cold zone and larger welding zone, the fracture toughness of the fitting increases.

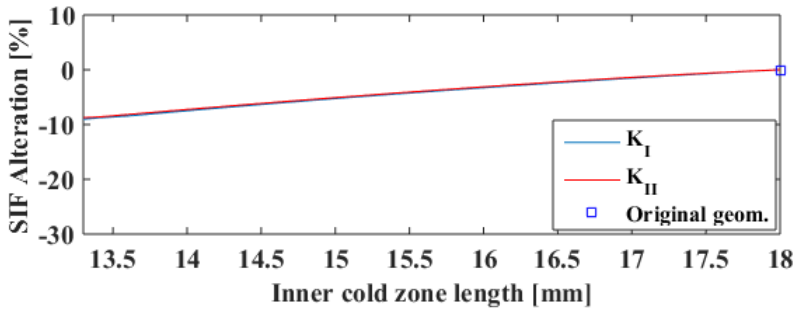

Figure 5.5: Relative difference of K_I and K_{II} as a function of inner cold zone length with a constant outer cold zone.

In the next step the outer cold zone varies and the welding zone and inner cold zone are respectively kept constant in two different cases. We name these cases Lin-Lout where the fusion length(Ls) is kept constant, Figure 5.6 and Ls-Lout where the inner cold zone length(Lin) is kept constant, Figure 5.7.

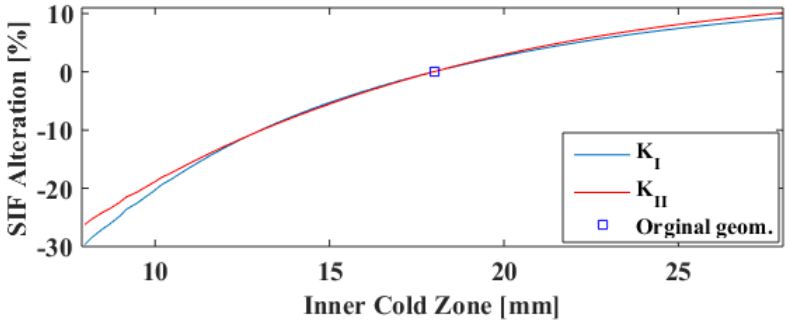

Figure 5.6: Relative difference of K_I and K_{II} as a function of inner cold zone length with constant fusion length.

From Figure 5.6,we can see that reducing the inner cold zone (crack mouth) will decrease the SIF values and increase the crack growth resistance. In the case with a constant inner cold zone (Ls-Lout),Figure 5.7, the results show minor trends that will be evaluated with the non-linear model.

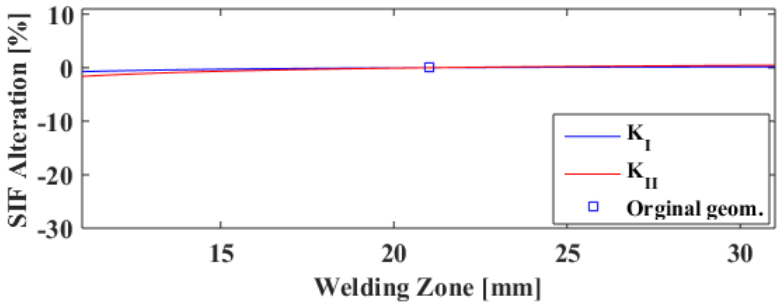

Figure 5.7: Relative difference of K_I and K_{II} as a function of fusion length with constant inner cold zone.

After studying the response to the changes of welding , inner cold zone and outer cold zone lengths with our load cases using the linear model, we can conclude that the length of the inner cold zone has the most important role in crack growth resistance of the EF fitting due to the direct relation to magnitude of the acting force on the crack and the crack opening force.

Effects of changing the EF fitting and pipe thickness on the outcome are shown in Figure 5.8. It can be noted that increasing the EF fitting thickness will improve the fracture toughness but increasing the pipe thickness has an opposite effect. When increasing both dimensions simultaneously, the total stiffness is increased and a decreasing SIF value can be observed but the improvement is not as significant as the first case where only the EF thickness was increased.

To complement these results, the displacements and deformation on the fitting and the pipe under effect of thermal and structural loads were studied. Due to the reason that the inside pressure is higher than the outside pressure, the fitting material experiences a rigid body motion which opens the crack. This motion forces the pipe material to move as well. When increasing the pipe thickness, the displacement of the fitting part meets more resistance and can not move the pipe part as before. The result of this change is a greater crack mouth opening (CMO) and therefore higher SIF values. An increase of the fitting thickness has an opposite effect. It increases the stiffness of the fitting and results in a force that opens the crack less than before, hence a decrease of SIFs magnitudes are seen in the outcome. Finally, the contribution of Young's modulus is studied, Figure 5.9. The HPDE material properties are temperature dependent as it was noticed and dealt with during the experiments. The temperatures inside or outside the pipe system can be different from the case that has been chosen and that leads to a difference in the Young's modulus magnitude. The Young's modulus at the fusion zone

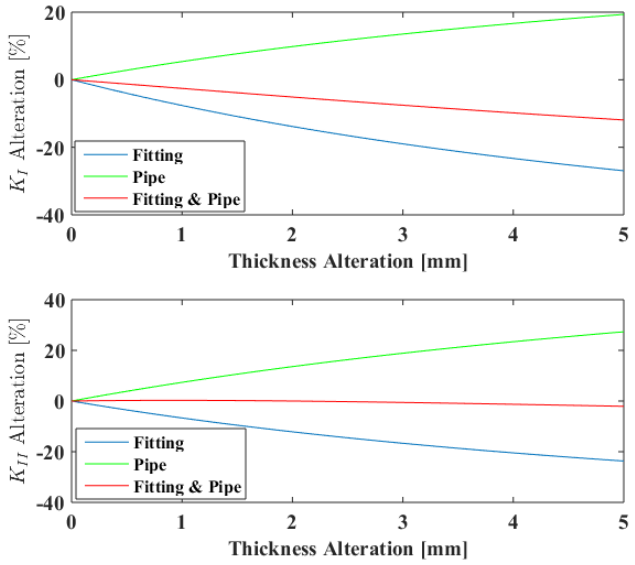

Figure 5.8: Relative difference of K_I and K_{II} as a function of joint thickness

is assumed to be the same as the HDPE material even though this value can change due to the crystallization of the material during the fusion process. Another reason for studying the effect of variation in Young's modulus is that this value can be different in pipe and fitting produced by different manufactures.

In Figure 5.9, SIF values decrease as the Young's modulus increases. There are two types of loading, one thermal and one structural. The structural load is a prescribed force and therefore not sensitive to change of E-value. A lower value leads to larger strains but the magnitude of stresses will be the same and SIFs are proportional to the stress value at the crack tip. When the thermal load is applied with higher E-value we are getting higher SIFs. Another result is that with the thermal load (4 °C at the outside and 10 °C at the outside) the resulting structural stresses closes the crack mouth. The super position of these two load cases leads to a decrease of total SIFs magnitudes. It can be noticed that two values of Young's modulus gathered in 25 and 10°C contribute to K_I magnitudes that differs around 6% from each other. Beside the temperature, there are other factors like welding process and different manufacturers that can result in a change in Young's modulus. Therefore it is important to have knowledge about the sensitivity of joining to this material parameter.

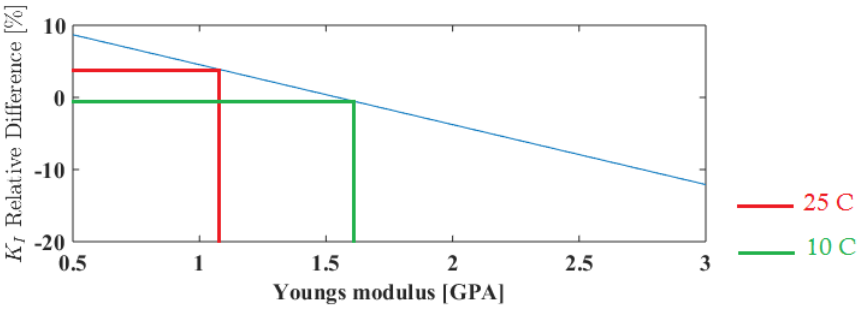

Figure 5.9: Relative difference of K_I and K_{II} as a function of Young's modulus.

5.1.5 Thermal loads effect

There are two types of loading in the linear model, thermal and structural. Before proceeding with non-linear model we studied whether the thermal load has a significant influence or not. SIF values are again calculated as the fusion length increases and the inner cold zone decreases (same as Figure 5.5) but this time without the thermal load. The relative difference shows that the thermal load induces a closing effect on the crack mouth, although the difference is relatively small.

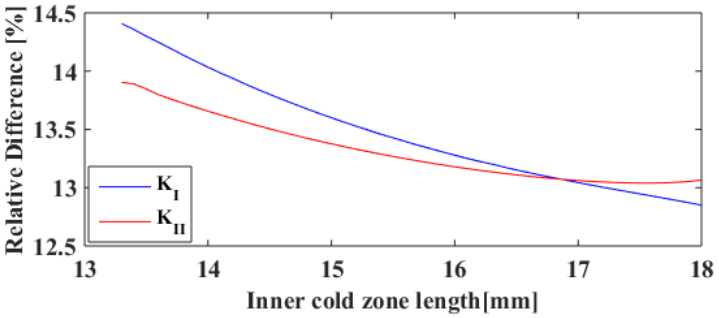

Figure 5.10: Relative difference in SIF with and without thermal loading as the inner cold zone length decreases with a constant outer cold zone length.

From this result we concluded that excluding the effect of the thermal load will not influence the results considerably and, furthermore, makes it more conservative by over estimating the critical load value. Therefore, we will not consider thermal load in subsequent analyses.

5.1.6 Conclusions of the LEFM analysis

Here is a summary of the conclusions from the results of the linear analyses.

- With the considered load cases, the stress-intensity factors in opening mode dominate (mode I), K_I .
- Copper wires located near the crack tip can affect the stress intensity factors.
- The inner cold zone is the dominating length parameter of the fitting. Decreasing the cold zones (smaller crack mouth in the case of prescribed force case) will improve the fracture toughness and reduce the value of stress intensity factors.
- Crack mouth opening CMO is caused by deformation and displacement of the fitting due to the inside pressure and increasing the thickness of the fitting improves the fracture toughness but increasing thickness of the pipe has the opposite effect.
- The thermal load with the chosen temperatures counteracts the inner pressure and closes the crack, Figure 5.10.
- An increase in magnitude of Young's modulus will decrease the SIF values in both mode I and mode II. This effect is due to the proportionality of effect of the thermal load (prescribed displacement) and Young's modulus. This result has implications in case of temperature change, which affect the elastic properties of the material.

5.2 Results & conclusions of the non-linear simulation

In order to compare the results in the parametric studies using the non-linear models, we recorded the inner pressure that leads to crack initiation. This pressure will be referred to critical load. The parameter study with the non-linear model is only focused on the geometric parameters.

5.2.1 Geometric parameter study of the CZM model

In Figure 5.11 - 5.13 we present the effect of fusion length (Ls), inner cold zone (Lin) and outer cold zone (Lout) on the critical load magnitude. The total length will be kept constant similar to the linear parameter study. In all the figures, we will indicate the nominal load level with a red line. If the critical load is below the red line, the fitting will fail with current geometries. The original, reference geometry is also shown the in the figures.

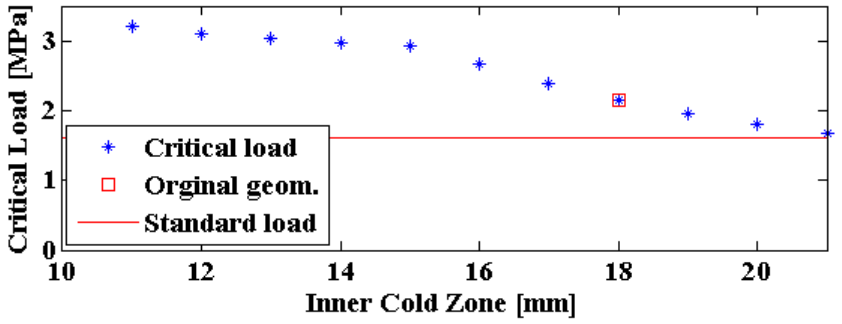

Figure 5.11: Critical load as a function of the inner cold zone length (Lin).

In Figure 5.11 we show the results from varying inner cold zone and fusion length. Decreasing the inner cold zone length (smaller crack mouth) increases the value of the critical load and improves the crack growth resistance.

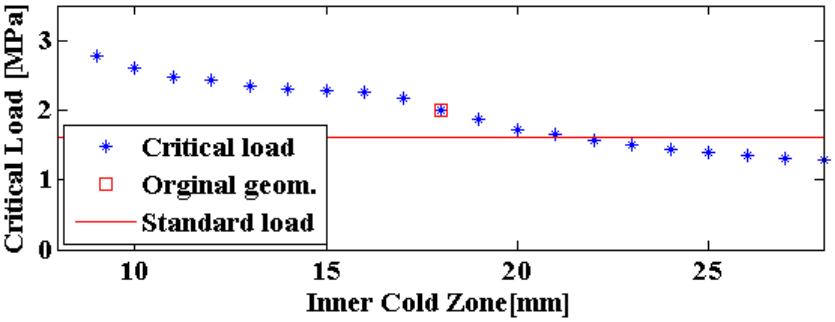

Figure 5.12: Critical load as a function of the inner cold zone length (Lin).

Figure 5.12 presents the results of varying both cold zone lengths with a constant fusion length that once again shows that decreasing the inner cold zone improves the fracture toughness and increases the critical load.

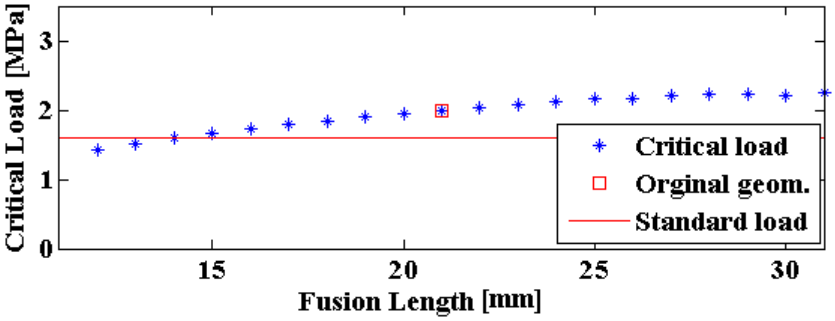

Figure 5.13: Critical load as a function of the fusion length (Lin).

The results of the linear model showed rather small influence of the fusion length (with a constant inner cold zone). In Figure 5.7, the results of the non-linear model shows that increasing the fusion length improves the crack growth resistance and decreasing this length lowers the critical load magnitude.

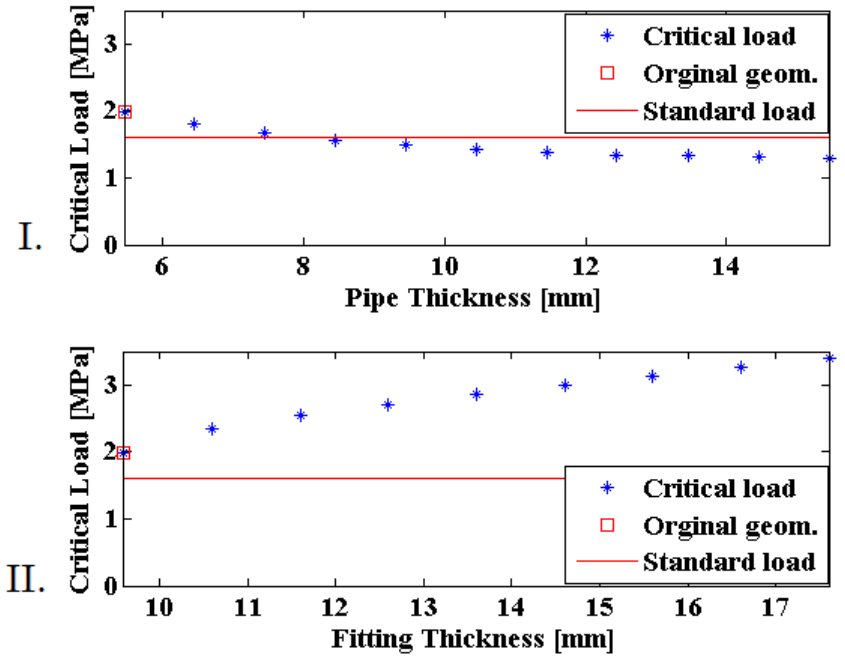

Figure 5.14: Critical load as a function of the pipe thickness (I) and fitting thickness (II).

The results of the pipe and fitting thickness effect on the critical load value are presented in Figure 5.19. Similar to the results on the linear parameter study, we can see that greater fitting thickness improves the fracture toughness and increases the critical load value, however increasing the pipe thickness has the opposite effect.

5.2.2 Conclusion of the CZM model

The conclusions of the non-linear CZM model are:

- The results of the CZM model are consistent with linear model.
- An increase of the fusion length will improve the crack growth resistance.
- The original geometry of the fitting with material parameters gathered from the experiments for an unsuccessful weld will hold where the critical pressure is higher, with a small margin, than the nominal/standard pressure.

5.2.3 Geometric parameter study of the XFEM model

In the XFEM model, the crack path is not predefined and can be predicted by the model. Using this model we found that once the interface is strong enough, the crack does no longer grow along the fusion zone but propagates upwards as it is presented in Figure 5.15.

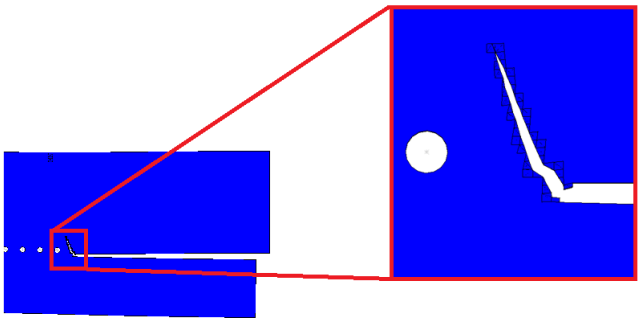

Figure 5.15: The crack path calculated with XFEM model.

With the material parameters for successful welding, the crack requires significantly greater inner pressure to initiate the crack opening. In Figure 5.16 the critical load as function of inner cold zone is presented where the outer cold zone is kept constant and only the inner cold zone and fusion length are varying.

Smaller inner cold zone length (crack mouth) improves the fracture toughness in this case as well. A similarly trend is observed when the fusion length is kept unchanged and the cold zones length is altered, Figure 5.17.

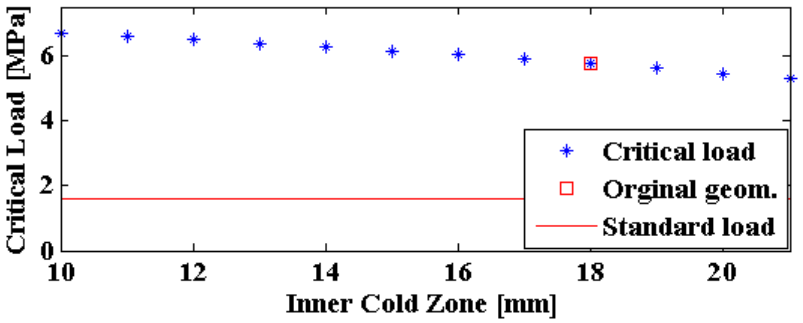

Figure 5.16: Critical load as a function of the inner cold zone length.

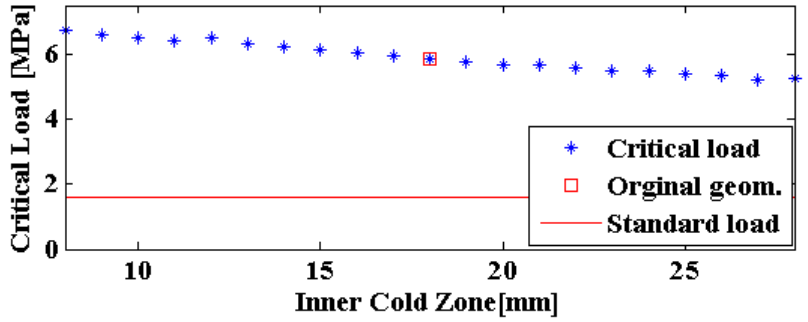

Figure 5.17: Critical load as a function of the inner cold zone length.

Similar to the CZM model, increasing the fusion length with a constant inner cold zone improves the crack growth resistance and increases the critical load value, Figure 5.18.

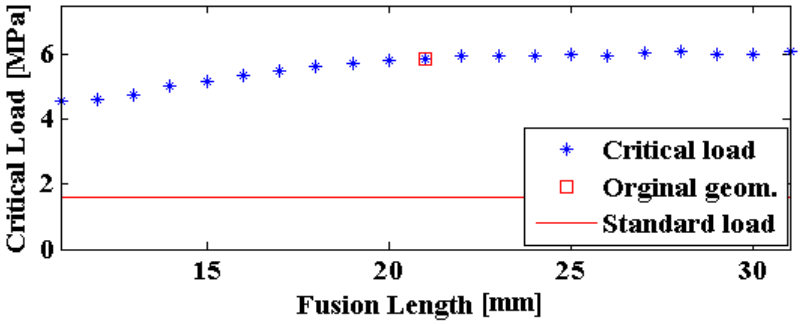

Figure 5.18: Critical load as a function of the fusion length.

The contributions of the altering thicknesses on the critical load value are slightly different from the results of unsuccessful welding with CZM. In the case of successful welding with XFEM model even an increase in the thickness of the pipe is improving the fracture toughness and increases the critical value. This result has to do with the direction of the crack which is not along the fusion line in this case.

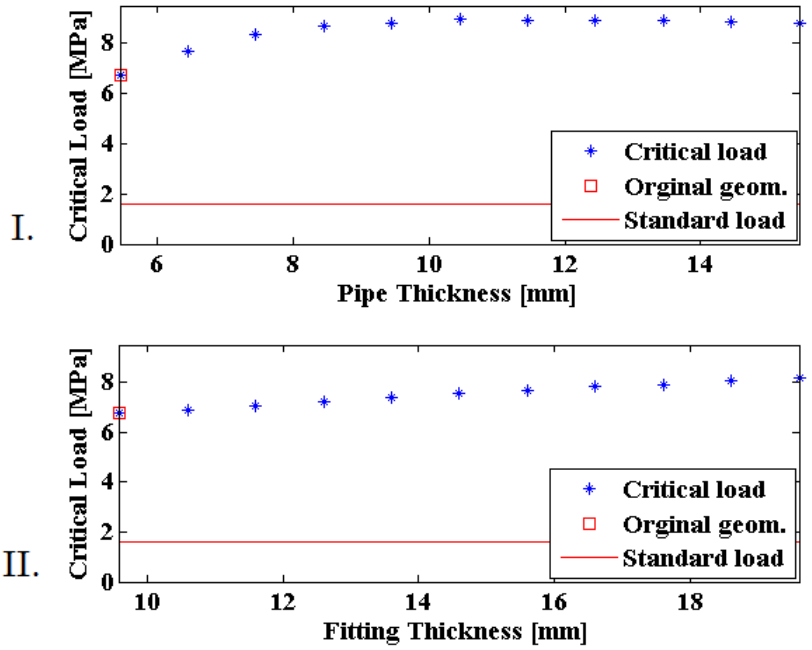

Figure 5.19: Critical load as a function of the pipe thickness (I) and fittng thickness (II).

5.2.4 Conclusions of the XFEM model

The conclusions of the non-linear XFEM model are:

- The crack propagates upwards with the strong interface.
- The welded structure has a critical load significantly greater than the nominal value.
- All the results except the contribution of the pipe thickness are consistent with the linear and CZM model. In the case of successful welding and the initial crack direction an increase in pipe thickness improves the crack growth resistance.

5.3 Final conclusions

By summarizing the results and conclusion from the linear, CZM and XFEM model, we can formulate our final conclusions.

The load cases, structural and thermal, applied on the joint resulted in an opening of the crack mouth that is the inner cold zone. The inside pressure is the dominating load that opens the crack and can be sufficiently large to cause failure, particularly with improper welding. The thermal load specified according to the reported standards (10 °C inside and 4 °C outside) and the outer pressure counteract the inner pressure and have a closing effect on the crack.

Both the linear fracture mechanics model and the non-linear model used for improper welding showed the same trends in response to the geometrical changes. The advantage of the non-linear model is its ability to predict the critical load.

The numerical studies performed with the material properties representing improper welding interface showed that the critical pressure is slightly above the nominal pressure used in the pipe, which means that the risk of failure is critically large. Decreasing the inner cold zone and increasing the fitting thickness has the greatest positive effect leading to an increased critical load and therefore minimized risk of failure. At the same time, the fusion length varied without reasonable ranges has a negligible impact on the risk of failure with poor welding interface.

With the parameters measured for the proper welding interface, the numerical studies showed that the crack does no longer propagate through the fusion zone, but rather develops toward the outer surface of the fitting, i.e. away from the pipe. The critical value of the inside pressure for the original geometry is about 4 times greater than the nominal pressure. Despite that, the parameter study showed similar trends observed for the improper welding interface, with both the decreased inner cold zone and the increased fitting thickness having the greatest positive impact on the crack opening load. In this case, however, increasing the pipe thickness also improved the crack growth resistance.

Bibliography

[1] *PE100 Pipe system.* Heiner Brömstrup, 2008.

[2] *A Review of the Electrofusion Joining Process for Polyethylene Pipe Sysytem.* Polymer engineering and science, 1997.

[3] *Analysis of Energy Balance When Using Cohesive Zone Models to Simulate Fracture Processes.* Journal of Engineering Materials and Technology, 2002.

[4] *The Creep and Fracture Behaviour of the Polyethylene PE100.* ETrans Tech Publications, 2014.

[5] *Defects Classification and Failure Modes of ElectrofusionJoint for Connecting Polyethylene Pipes.* Journal of Applied Polymer Science, 2012.

[6] *SS-EN 12201:3 2011.* Swedish Standard Institute.SIS, 2012.

[7] *Modelling large deformation behaviour under loading–unloading of semicrystalline polymers: Application to a high density polyethylene.* International Journal of Plasticity, 2010.

[8] *Schaktfritt byggande av markförlagda VA-ledningar av plast.* Svensk Vatten, 2010.

[9] *Plaströr för allmänna VA-ledningar.* Svensk Vatten, 2008.

[10] *Material Mechanics.* Department of solid mechanics,KTH Engineering Sciences, 2006.

[11] *Extended Finite Element Method.* International Jornal for Numerical Methods in Engineering, 2011.

[12] *Fracture Mechanics from Theory to Applications.* Department of solid mechanics,KTH Engineering Sciences, 2006.

[13] *Testing Techniques in Solid Mechanics.* Department of Solid Mechanics, KTH, 2012.

[14] *Engineering Manual for Piping systems.* SIMONA, 2010.

[15] *Effect of temperature on tensile properties of HDPE pipe material.* Institute of Materials, Minerals and Mining, 2006.

Appendices

A Creep law

A body under prescribed force will have a deformation that will follow the Eq. 2.1 at first but afterwards there will be another type of deformation as a function of time. This phenomena is called creep. The creep strain contains three parts, primary, secondary and tertiary creep. We have chosen to include the first two part. The primary and secondary creep of the HDPE is estimated by a combined time hardening model with a general formulation presented in Eq. 2.

$$\epsilon_{creep} = C_1 \sigma^{C_2} t^{C_3+1} \frac{e^{-\frac{C_4}{T}}}{C_3+1} + C_5 \sigma^{C_6} t e^{-\frac{C_7}{T}} \tag{2}$$

An earlier study on creep behaviour of HDPE,[4], provided the values needed to calculate the constants in Eq. 2. The primary and secondary creep are presented in Figure 1.

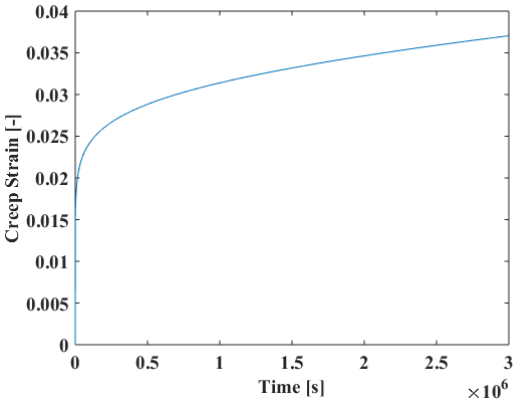

Figure 20: Primary and secondary creep,[4].

Since the thermal load is omitted, the temperature dependent part of Eq. 2 was removed and constants C_4 & C_7 will be set to zero. Remaining constants are calculated

and presented in Table 1 from an earlier study on this material.[4]

Table 1: Constants for HDPE creep law

Name	Value	Name	Value	Name	Value
C_1	$7.64 \cdot 10^{-7}[MPa^{-5}s^{-0.1}]$	C_2	5 [−]	C_3	−0.9 [−]
C_4	0 [°C]	C_5	$4.25 \cdot 10^{-12}[MPa^{-4}s^{-1}]$	C_6	4 [−]
C_7	0 [°C]	-	-	-	-

It should be noted that values in Table 1 are calculated in a $[MPa \ \& \ mm]$ unit system.

B Tomography

Tomography is one of the techniques for making a detailed x-rays of a plane section of a solid object suitable for 3D reconstruction. Waves are sent though the object and a computer produce images of the cross section by interpreting the information on how the waves are changed. This is a very suitable technique for investigating objects without destroying them.

It was decided to test this technique on an unsuccessful we ld in this project. The expectation was to see the discontinuities in the fusion zone to characterize the welding interface. The waves used for HPDE and other plastic materials needed to have a low frequency in order to be able to capture any image. However this kind of waves shatters easier than high frequency waves.

Unfortunately the apparatus available for this experiment could not provide any useful information in order of characterization of the welding zone. The main reason is that the low frequency waves that are used shatter when they hit the copper wires of the EF fitting. The images before and after the waves hit the copper wires are presented in Figure 21. This limitation made the imaging results useless for the analysis.

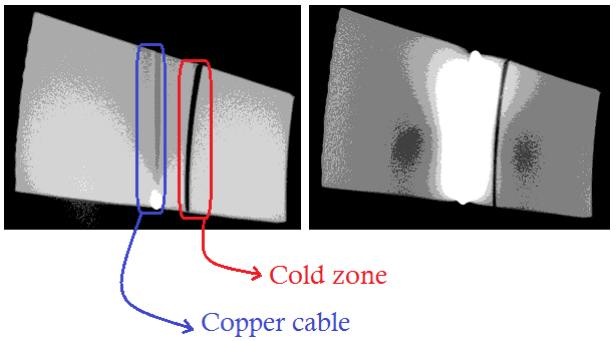

Figure 21: Tomography images of an unsuccessful EF fitting where low frequency wave shatters after hitting the copper wires.

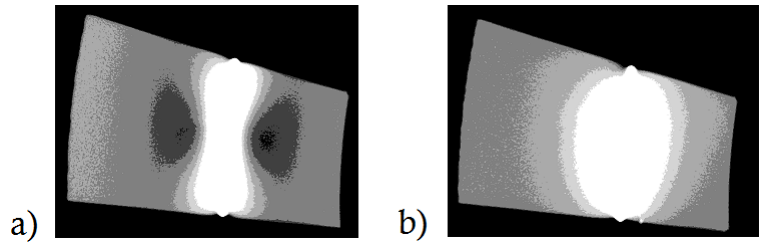

Figure 22: Tomography images of two different cross section of an unsuccessful EF fitting.